Journal of Sol-Gel Science and Technology (2020) 96:287–296
https://doi.org/10.1007/s10971-020-05410-z

ORIGINAL PAPER: FUNCTIONAL COATINGS, THIN FILMS AND MEMBRANES (INCLUDING DEPOSITION TECHNIQUES)

Preparation of mesoporous silica thin films at low temperature: a comparison of mild structure consolidation and template extraction procedures

Gustavo Giménez[1] · Gabriel Ybarra[1] · Galo J. A. A. Soler-Illia[2]

Received: 24 June 2020 / Accepted: 31 August 2020 / Published online: 17 September 2020

Abstract

Mesoporous thin films (MTFs) displaying high surface area and controlled porosity constitute interesting materials for a plethora of applications in optics and electronics. A critical aspect in MTF processing is template removal that usually consists in thermal treatment at 350 °C, which consolidates the oxide film but might change the pore features. In addition, the use of such high temperature must be avoided when organic functionalities are to be preserved, or in the case of film deposition on polymeric substrates. Here we present and compare five different methods to consolidate silica MTF (SMTF) in mild conditions, at a maximum processing temperature of 130 °C. Conditions, such as duration of the thermal treatment, vacuum conditions, exposure to acidic and alkaline media, were systematically explored and the resulting films were analyzed by optical microscopy, focused ion beam, scanning electron microscopy, ellipsometry, and infrared spectroscopy. The optimized conditions leading to accessible mesopores and a stable oxide structure that can be used as a mesoporous perm-selective electrode are discussed.

Graphical Abstract

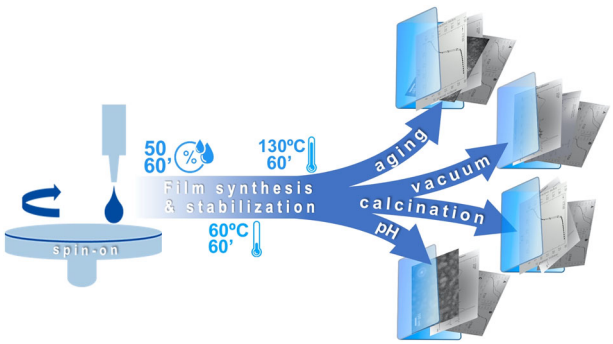

Keywords Mesoporous thin films · Soft processing · Sol–gel condensation · Template extraction

Supplementary information The online version of this article (https://doi.org/10.1007/s10971-020-05410-z) contains supplementary material, which is available to authorized users.

✉ Galo J. A. A. Soler-Illia
gsoler-illia@unsam.edu.ar

[1] INTI-Micro y Nanotecnologías, Instituto Nacional de Tecnología Industrial, Av. Gral. Paz 5445, San Martín, Buenos Aires, Argentina

[2] Instituto de Nanosistemas, Universidad Nacional de San Martín, CONICET, Av. 25 de Mayo 1021, San Martín, Buenos Aires, Argentina

Highlights

- Soft template extraction methods from mesoporous silica thin films onto Si and Au were compared.
- These low-T treatments permit to extract ionic and non-ionic surfactants, keeping film integrity.
- A complete analysis on template extraction, film adhesion, and mesopore size is provided.
- Optimized 130 °C treatment followed by vacuum leads to robust frameworks with accessible mesopores.
- Mesoporous electrodes can be used for more than 90 consecutive electrochemical cycles in aqueous solutions.

1 Introduction

Mesoporous thin films (MTFs) have attracted the interest of the scientific community in the last two decades, due to their multiple applications in sensors, (photo)catalysts, molecular sieves, etc. [1] These materials are synthesized by the combination of sol–gel chemistry and self-assembly of supramolecular templates [2, 3]. In particular, silica mesoporous thin films (SMTFs) have been intensely studied for the flexibility of organosilicon chemistry, with a huge potential of surface modification. Indeed, SMTF constitute an excellent matrix to introduce molecular functionalities, especially for the development of sensors, drug encapsulation and delivery, and electronic tongues [4–6].

The functionality of MTF is determined by the degree of condensation of the oxide, the efficiency of template extraction, and the resulting porous structure. SMTF with a high degree of consolidation lead to more compact structures with a lower content of silanol groups. A complete extraction of the template is also relevant, particularly if the films are to be used in size-selective filters, preconcentrators, or catalysts [7–10].

In order to obtain an adequate control and stability of the final structure, the inorganic framework templated by the micelle arrangement must be stabilized before calcination. Typically, a low thermal treatment at around 130 °C is carried out toward this end [11, 12]. Subsequently, another thermal treatment, typically between 350 and 600 °C, is commonly used to further consolidate the oxide film and remove the organic template by calcination [13–15].

In many MTF systems, there is considerable interest in removing the template without degrading all the organic components; for instance, in those MTF deposited on flexible polymeric substrates, or in hybrid organic–inorganic frameworks, in order to preserve organic modifications introduced during the sol–gel synthesis. In the last years, several methods to obtain SMTF have been reported avoiding calcination. As early as in 2000, Clark et al. [16] used UV radiation (187–254 nm) to generate an oxidizing, ozone-rich atmosphere to remove the surfactant. The method was applied successfully on silica films structured with Brij56, although the arrangement of pores changed from hexagonal to cubic after UV exposure. In the same year, Hozumi et al. [17] reported a photocalcination method applying vacuum and UV radiation (172 nm) to partially remove the template in SMTF structured with cetyltrimethylammonium chloride. The works of Huang et al. [18] and Zhang et al. [19] used plasma to remove the template. The former used oxygen plasma on TiO_2 MTFs and the latter adapted the method to be used on silica-based mesoporous with argon plasma. Both works concluded that this treatment led to structural disorder and changes in the degree of porosity, and control over the final structure was unpredictable. Horiuch et al. [20] proposed a photocatalytic process to remove the surfactant. They modified the surface of SMTF with TiO_2, irradiated with a UV source and concluded that TiO_2 was actively involved in the oxidation and removal of Brij78, which was used as a template. They used unmodified SMTF as a control experiment and under these conditions they observed no evidence of surfactant removal. Template extraction and film consolidation have been carried out using acidified ethanol as a solvent at 200 °C. This temperature was chosen to promote the condensation of the inorganic phase without compromising the integrity of the organic functionalities incorporated in the films.

In spite of all these previous investigations, a comparative study is still lacking in the specialized bibliography about the effect of different treatments at low temperatures on the consolidation degree of the silica films, the template extraction, and the porous structure of the resulting mesophases.

The methods mentioned in the previous paragraph as alternatives to heat treatment seem promising. However, they present some limitations in their application. Plasma is difficult to control and the penetration into MTFs is low. Removal with UV radiation is restricted to photodegradable surfactants or requires assisting the oxidation of the template with some photoactive modification.

In this work, in order to further advance in the development of mild methods for SMTF processing, different processes and conditions were explored to condense the inorganic oxide and extract the organic template in SiO_2 MTFs at low temperatures (130 °C). The treatments were aimed at producing SMTF with accessible porosity and a condensed, robust framework, and were performed on the same pristine mesostructured silica films, therefore permitting a better comparison between soft template removal methods in crucial aspects for SMTF such as the generation of open porosity and mesostructure stability. We prove that the SMTF prepared under these mild conditions can be used as perm-selective membranes in electrochemical devices.

2 Experimental

2.1 Sol preparation

Pluronics F127 triblock copolymer (Sigma-Aldrich) and cetyl trimethyl ammonium bromide (CTAB) were used as the pore templating agents, and tetraethoxysilane was employed (TEOS, Merck) as the oxide precursor. A mixture of absolute ethanol (Biopack) and E-pure or Milli-Q water (18 MΩ cm^{-1}) was used as solvent. HCl (Merck) was used to control the hydrolysis and condensation of the inorganic species. Mesoporous silica thin films were prepared from two different sols with a molar ratio TEOS:EtOH:H_2O:HCl: F127 = 1:40:10:0.008:0.005 and TEOS:EtOH:H_2O:HCl: CTAB = 1:40:10:0.008:0.1, in order to obtain films with an *Im3m* cubic mesostructure with 8 nm pore diameter [21], and a 3D hexagonal *P63/mmc* with 3 nm pore diameter, respectively [22]. The sols were aged at room temperature for 48 h prior to deposition to favor the hydrolysis of the inorganic precursor. The aged sols were deposited by spin coating (4000 rpm during 30 s) onto silicon and silicon/gold substrates at room temperature followed by a sequence of stabilization processes: aging in 50% RH controlled atmosphere for 60 min, 60 °C for 60 min, and 130 °C for 60 min [11, 23]. In order to obtain mesoporous films onto gold electrodes, SMTFs were deposited onto sputtered gold electrodes (Ti|Au 10|100 nm, Targets 3N) on top of silicon wafers (University Wafer, Inc.). Gold-coated silicon wafers were treated with MTMS (3-mercaptopropyl trimethoxysilane 95%, Sigma-Aldrich) prior to deposition in order to improve the adhesion of the mesoporous silica films [24].

The different methods used for extraction and consolidation are summarized in Table 1. In the high temperature method (HT), which follows the most used protocol in the literature, samples were heated at 350 °C during 2 h using a ramp of 1 °C min^{-1}. In the alternative methods reported here, template removal was carried out after each treatment by refluxing samples in isopropyl alcohol during 15 min, followed by rinsing with a mixture of ethanol and water of pH = 2, which constitutes a mild and fast method.

Table 1 Description of methods employed after a previous stabilization treatment (50% RH for 60 min, 60 °C for 60 min, and 130 °C for 60 min)

Method	Description	Refs.
HT	Calcination: thermal treatment at 350 °C during 1 h (1 °C/min)	[2, 7, 25–28]
I	No further treatment	[25, 29, 30]
II	Heat treatment at 130 °C during 7 days	[31]
III	Heat treatment at 130 °C and high vacuum during 7 days	[32–34]
IV	Exposure to HCl fumes (15 min)	[13, 35–38]
V	Exposure to NH_3 fumes (15 min)	[36, 37, 39, 40]

After applying Methods I–V, template extraction was carried out with isopropanol followed by rinsing with diluted HCl

2.2 Films characterization

Refractive indexes and thicknesses of silica films (Si substrate/SiO_2 mesoporous layers) were measured after surfactant extraction by spectroscopic ellipsometry (SE SOPRA GES5A). A Cauchy dispersion law for transparent materials was used to model the films thickness and the complex refractive index $n(\lambda) = n(\lambda) + i\ k(\lambda)$ [41, 42]. Environmental Ellipsometric Porosimetry Analysis (EPA) was also performed, in order to obtain the mesopore fraction and pore size distribution through water adsorption–desorption isotherms. Pore volume and diameter were calculated from these isotherms using the Winelli II software [43]. Samples were observed with an Olympus BX50 optical microscope to assess the homogeneity of the films and scanning electron microscopy was used to characterize the surface structure of pores. Thicknesses were also measured by SEM after cross-sectioning by FIB, using a FIB/SEM Microscope (Thermo Fisher Helios NanoLab 650). Statistics ($N = 50$/image) and fast Fourier transforms (FFT) were carried out with ImageJ. The infrared spectra were acquired with a Nicolet 6700 Fourier transform infrared spectrometer. Template extraction was calculated as the ratio of the areas of the ν_{C-H} bands (2800–3000 cm^{-1}) before and after the extraction process. The contact angle measurement was carried out on a Ramé-Hart 290 instrument and analyzed with DROPImage software.

Substrates for the electrochemical measurements consisted in gold thin films deposited onto silicon wafers by sputtering. SMTFs were subsequently deposited on these substrates by using Methods HT and III. Cyclic voltammetry experiments were carried out with a Teq_04 potentiostat in a three-electrode electrochemical cell, using a saturated calomel electrode as reference electrode and a Pt foil as counter electrode. The exposed area of working was limited to a circle of 2 mm in diameter. Electrochemical measurements were performed at 0.05 V s^{-1} in solutions prepared using deionized water (18 MΩ cm^{-1}) containing 0.1 mM $Ru(NH_3)_6Cl_3$ (Sigma-Aldrich) or 1 mM $K_4Fe(CN)_6.3H_2O$ /1 nM $K_3(CN)_6.3H_2O$ (Sigma-Aldrich) and 0.1 M KCl (Biopack).

3 Results and discussion

The alternative methods to thermal treatment at 350 °C presented here were inspired by previous works to obtain robust, homogeneous mesoporous oxide films with a high

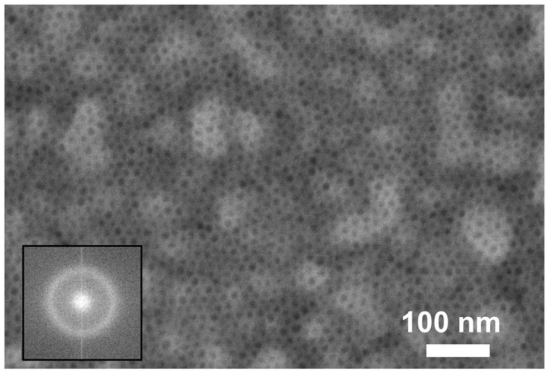

Fig. 1 SEM of F127-structured mesoporous silica thin film with the associated FFT pattern (inset)

degree of condensation and template removal at 130 °C [18, 31, 44–46]. A completely condensed film was prepared by calcination with the aim of comparing the efficiency of the alternative methods. Homogeneous films without cracks were obtained by this classical synthesis method.

The adsorption isotherms and the distribution and size of pores and necks were similar to those presented in previous works [2]. EPA analysis showed a high porosity in the films (42% and 38% for CTAB and F127, respectively) with type IV adsorption isotherms and H1/H2 hysteresis loops, in accordance with mesoporous materials with interconnected pores and necks systems. The hysteresis shape and distribution indicate the presence of pores and necks of uniform sizes as previously reported [47] (Online Resource S1). The isotherm, the SEM image, and its FFT pattern (Fig. 1) of the film obtained using F127 as template were in accordance with a *Im3m* cubic mesostructure with 8 nm pore diameter [21], while the isotherm for the CTAB porous system suggests a 3D hexagonal *P63/mm* structure [48]. The results presented for calcined systems were used as a reference of a totally porous and consolidated silica framework to compare with the alternative developed methods. The films obtained with the different mild template removal methods were systematically characterized and the results are summarized in Table 2. A brief discussion of the most relevant results for each of the alternative methods follows.

3.1 Methods I–III: influence of aging and vacuum in the preparation of the films

A series of treatments were carried out in which the condensation time at 130 °C was extended for 0, 1, 2, 5, or 7 days under atmospheric pressure and 7 days under high vacuum. In all cases, homogeneous thin films with high adhesion to the silicon substrate were obtained after this treatment, both for F127 and CTAB templates. When CTAB was used as a template, films with well-defined

Table 2 Summary of characterization of films prepared with different methods

Method	Template	Extraction (%)	Distribution of necks	Adherence to silicon	Adherence to gold	Pore diameter (nm)	Neck diameter (nm)	Porosity (%)	Refractive index	Thickness (nm)	Contact angle (°)	Type of isotherm and hysteresis
Calcination	F127	100	Single	Excellent	Good	8.2	4.4	38	1.391	207	20	IV/H1–H2
	CTAB	100	Single	Excellent	Poor	2.5	2	42	1.384	265	33.2	IV/H1–H2
I	F127	70	Double	Excellent	Good	7.5	3.9[a]	30	1.390	211	36.4	IV/H2
	CTAB	73	Single	Excellent	Fail	2.2	2	30	1.389	308	41.2	IV/H5
II	F127	97	Double	Excellent	Good	8	4.0[a]	39	1.381	212	22.7	IV/H2
	CTAB	88	Single	Excellent	Fail	2.5	2	41	1.375	338	44.5	IV/H1
III	F127	88	Single	Excellent	Excellent	9	4	38	1.383	223	42.5	IV/H1–H2
	CTAB	88	Single	Excellent	Fail	2.2	1.7	44	1.393	381	65.5	IV/H2
IV	F127	86	Double	Excellent	Good	5.7	2.1	31	1.399	191	28.2	IV/H1–H5
	CTAB	92	Single	Excellent	Fail	2	1.6	37	1.386	340	46	IV/H1
V	F127	91	Double	Excellent	Good	8	2.1	32	1.374	225	24.5	IV/H1–H2
	CTAB	91	Single	Excellent	Fail	2.3	1.6	46	1.374	383	47.6	IV/H1

SD single neck distribution, *DN* double neck distribution

[a]Widest necks

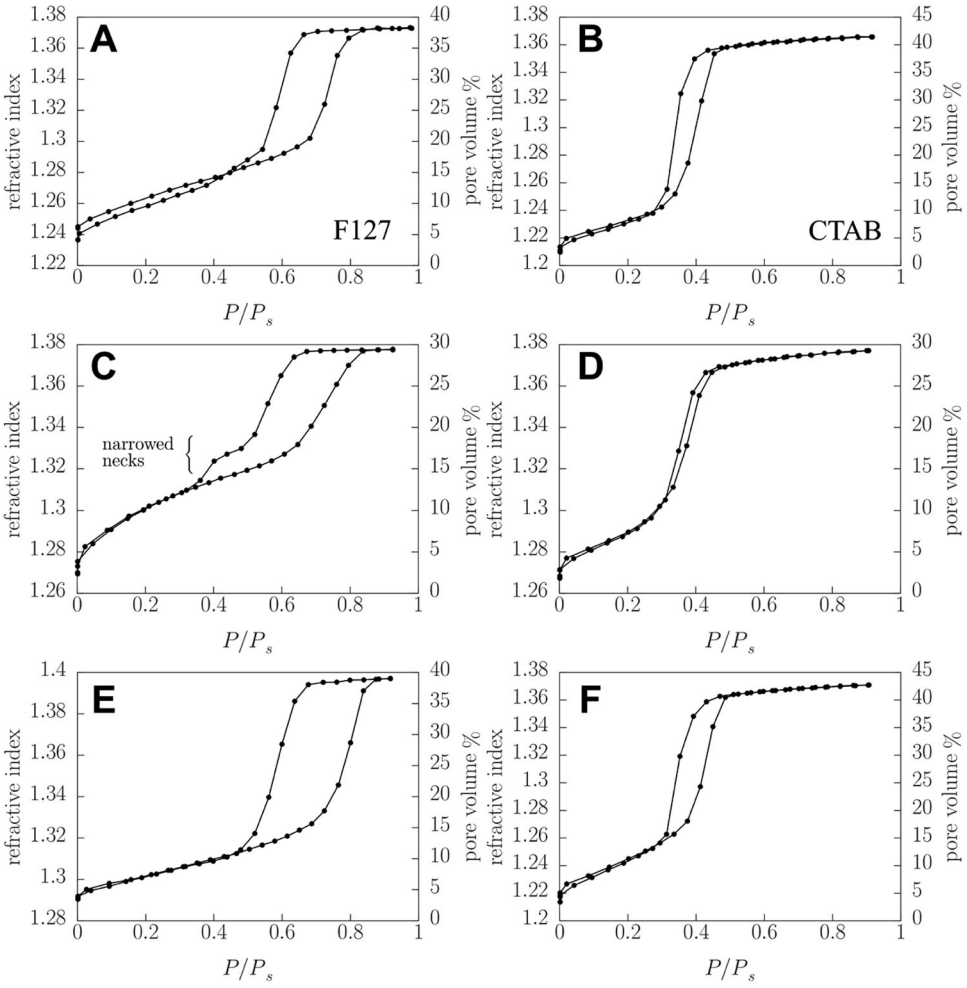

Fig. 2 Comparison of the adsorption–desorption isotherms obtained by ellipsometric porosimetry between the Methods I, III with calcined films. Mesoporous films with F127 template are shown in the left side and mesoporous films with CTAB template in the right one, for films obtained by calcination (**a**, **b**), by Method I (**c**, **d**), and by Method III (**e**, **f**)

pores and necks were obtained. However, a double distribution of necks was observed when F127 was used in Methods I and II (Fig. 2c). In those cases, ellipsoporosimetry showed that desorption occurs at two values of P/P_0. It has been proposed that this behavior is due to a partial occlusion of the pores. When desorption occurs through necks of different sizes, the driving force necessary to overcome the surface tension must be greater, therefore desorption takes place at lower P/P_0 values for smaller diameter of the pores according to the Kelvin equation [49–51]. This result suggests that this consolidation procedure leads to a system with a double distribution in the size of the necks, or two systems with different neck sizes that are not interconnected. In the case of CTAB, a small hysteresis can be observed, which indicates that the pores are partially blocked (Fig. 2d). Both results suggest that template extraction is incomplete for Method I, in accordance with the infrared spectra, from which an extraction of about 70% was estimated for both systems (Table 2).

For the Method III, high vacuum (10^{-5} mbar) was applied in order to remove volatile products from the sol–gel reaction (water and alcohol) and thus favor the condensation of the oxide [32]. The water adsorption/desorption curve for F127-structured films showed a type IV isotherm with H2 hysteresis, typical of systems with uniformly distributed monodisperse pores, reaching a refractive index of $n = 1.25$ at $P/P_0 = 0$ and a porosity of 38%, which are values close to those of a calcined film (Fig. 2e). For systems structured with CTAB, homogeneous films were also obtained without discontinuities or cracks. From EPA measurements (Fig. 2f), a porosity of 44% and a wall effective refractive index of 1.393 were obtained, very close to those of the calcined film, with a distribution of pores and necks size comparable to the reported by Boissiere [43, 40].

Figure 3 shows FTIR spectra of mesoporous films before and after template removal using the HT treatment. The C–H band (2950–2850 cm^{-1}) due to the surfactants was completely absent after calcination at 350 °C. Typical bands for the SiO_2 species can be observed in the spectra: $\nu_{Si–O–Si}$ (LO_3, 1250 cm^{-1}), $\nu_{Si–O–Si}$ (TO_3, 1170 cm^{-1}), $\nu_{Si–OH}$ (965 cm^{-1}), and $\nu_{Si–O–Si}$ (TO_2, 800 cm^{-1}) [45, 46]. It is worth mentioning the nature of the shoulder at 1180 cm^{-1} in the TO_3 band, which intensifies with increasing porosity, due to coupling of the longitudinal LO_3 and transverse TO_3

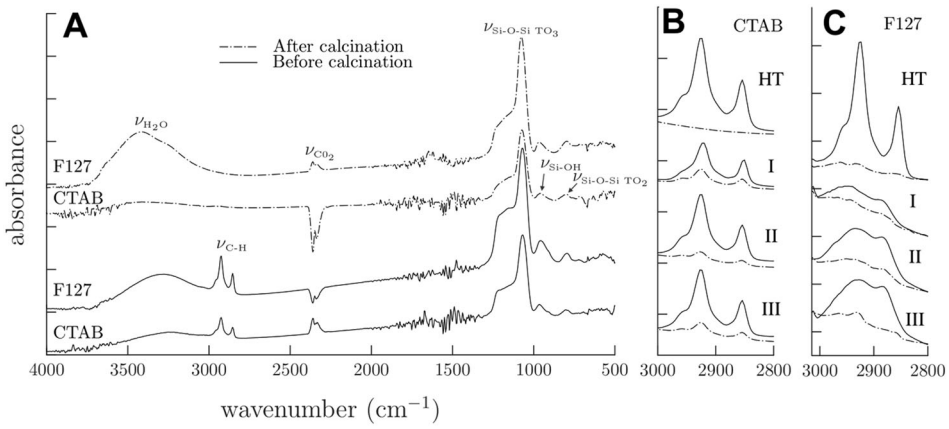

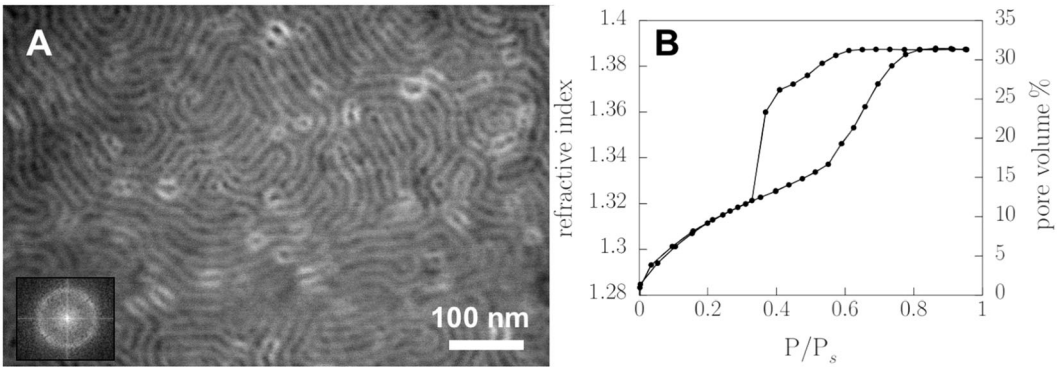

Fig. 3 FTIR spectra for porous systems obtained by calcinations (HT Method) using CTAB and F127 as a templating agent, before (solid line) and after (dotted line) template extraction **a**. Comparison of the C–H bands before and after template extraction for Methods HT and I–III using CTAB **b** and F127 **c**

Fig. 4 SEM image **a** and ellipsometric adsorption–desorption water isotherm **b** of films obtained using Method IV with F127 as a template agent

vibration modes, associated with the dispersion of the infrared radiation in the pores [47]. The results presented for calcined systems were used as a reference of a totally porous consolidated silica framework to compare with the alternative methods developed.

The FTIR spectra for Methods I–III (with CTAB and F127) are consistent with a consolidated mesostructure due the characteristic bands for SMTF present between 1200 and 1000 cm^{-1}, and it can be concluded that increasing the aging time promotes the template extraction. Although removal of the surfactant was not complete, a high level of extraction could be achieved in both cases, above 85% (Fig. 3).

3.2 Methods IV and V: influence of extreme pHs in the films synthesis

It has been reported [13, 34–39] that effective condensation of silica mesoporous films could be obtained at pH values lower than 1 and higher than 12. Strongly acidic medium (pH < 1) favors alkoxide hydrolysis and condensation of siloxane groups [13, 35–38] and highly alkaline media (pH > 12) promote the catalysis of the TEOS hydrolysis [36, 37, 39, 40].

In the present work, films stabilized at 130 °C were subsequently exposed to HCl and NH_3 fumes. The films were homogeneous for both templates. Scanning electron microscopy images of F127 systems show that the mesopores evolved to elongated pore systems, intermediate between an *Im3m* and a 2D hexagonal (*p6mm*) structure [39]. The observed structure shows a locally ordered mesostructure which is the result of a partial pore merging along the (111) directions of the body-centered cubic architecture. This change is attributable to the incompletely condensed hybrid framework and the evolution is facilitated due to the epitaxy relationships between the (111) axis of the cubic mesostructure and the long pore axis of the 2D hexagonal structures [52]. This surface morphology of elongated pores was corroborated by the water adsorption/desorption isotherm obtained by EPA, in which a double distribution of necks with large diameter predominates, with almost the same size as the pores, in accordance with the SEM images (Fig. 4). Water adsorption/desorption isotherm for films structured with CTAB showed a porosity of 38% and a refractive index of 1.23 at $P/P_0 = 0$, as in the case of F127 slightly higher than those of HT films. Infrared spectra showed that

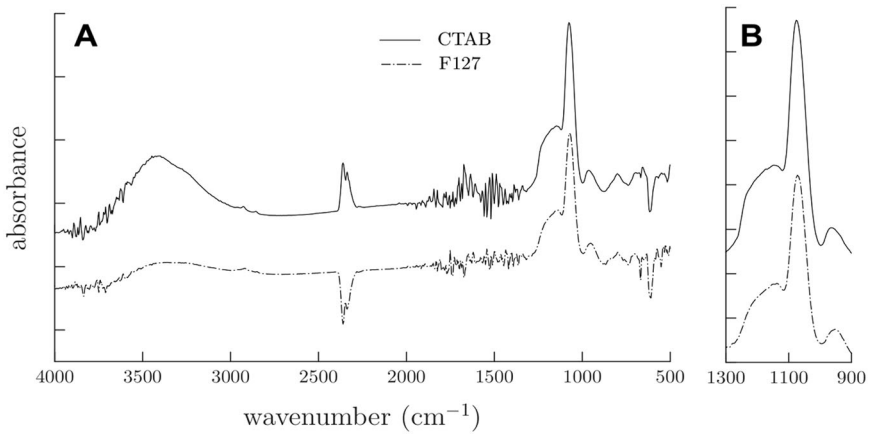

Fig. 5 Infrared spectra for porous systems obtained by exposure to ammonia fumes (Method V) **a**. An enhancement in band at 1170 cm^{-1} band (LO_3–TO_3 couplings) is observed suggesting a loss of order in the porous structure for both systems **b**

template extraction reached a value of 92% for CTAB and 86% for F127 (Table 2).

In the films that were exposed to NH_3 fumes for 15 min (after humidity and temperature stabilization), optical and electronic microscopies revealed homogeneous films, without cracks and with an excellent adherence to the silicon substrate with *Im3m* structure. EPA showed a double distribution of necks similar to that obtained with Method IV using F127 (Online Resource S2). However, in this case the refractive index was 1.22 at $P/P_0 = 0$, which is very close to the value obtained for calcined films. For films structured with CTAB, measurements by EPA showed a Type IV isotherm, with H1 hysteresis, resulting in a highly porous system (40%) and a refractive index of 1.22 at $P/P_0 = 0$. The infrared spectra for both surfactants (Fig. 5) showed an atypical shoulder (LO_3–TO_3 coupling, at 1180 cm^{-1}) for mesoporous silica structures [53–55]. This suggests a change of the pore organization in the nanoscale, due to the partial dissolution of the silica, catalyzed by the alkaline medium. While the basic medium accelerates the hydrolysis of TEOS, it also increases the dissolution rate of SiO_2 [56–59]. It has been reported [54, 60–62] that the enhancement of the band at 1170 cm^{-1} can be interpreted as an increase in the tension of Si–O–Si bonds and thus be indicative of an increased disorder in the micropore structure. This result is in accordance with the EPA measurements, which showed a widening of the necks to almost the same size as the pores, as can be seen in Fig. 4 for films prepared with F127 treated with acidic fumes.

Summing up, it could be observed that all the methods presented here were effective to obtain mesoporous films with accessible pore systems, without any discontinuity or cracks for both template agents, F127 (Online Resource S3) and CTAB. The calculated effective refractive index showed a deviation of <2% from those films obtained by calcination, in accordance to those reported in the literature [63–67], suggesting a good condensation of the inorganic phase.

However, dissimilar results were obtained regarding to the porous structure and template extraction for the different methods. Films treated at 130 °C during as long as 7 days presented a double distribution of necks when F127 was used. When this treatment was aided by vacuum, a single distribution of pores and necks was obtained. Finally, the use of acid and alkaline fumes produced a modification in the structure of the pores.

With respect to the template extraction, FTIR spectra showed that surfactants were effectively removed by calcination. A treatment with an acidic alcoholic solution showed an average 90% efficiency of template extraction for most of the low-temperature treatments, with the exception of Method I in which a 1-h treatment at 130 °C was used. Longer treatment times at the same temperature favored the process of template removal.

Adhesion to the electroactive substrate, pore accessibility and stability in solutions are critical factors in SMTF applications. In order to test the usefulness of the consolidation–extraction procedures reported here regarding these features, SMTF were processed and tested as permselective electrodes. In all cases, SMTF presented excellent adhesion to Si wafers, as expected, due to the chemical compatibility of the substrate and the film composition; films did present a continuous crack-free structure and withstood immersion in aqueous solutions. However, SMTF deposited onto gold substrates presented a variable degree of adhesion, reflected in the formation of cracks on the surface even when the gold thin films were treated with 3-mercaptopropyl trimethoxysilane to improve the chemical compatibility of the interface. When F127 was used as a templating agent, adhesion of SMTF to gold varied from good (no cracks observed, but sample-to-sample partial detachment when immersing in solutions) to excellent (all samples stable when exposed to solution). On the other hand, CTAB-templated films presented poor adhesion and large detached areas of the films could be observed over gold substrates (Online Resource S4). Poor adhesion of

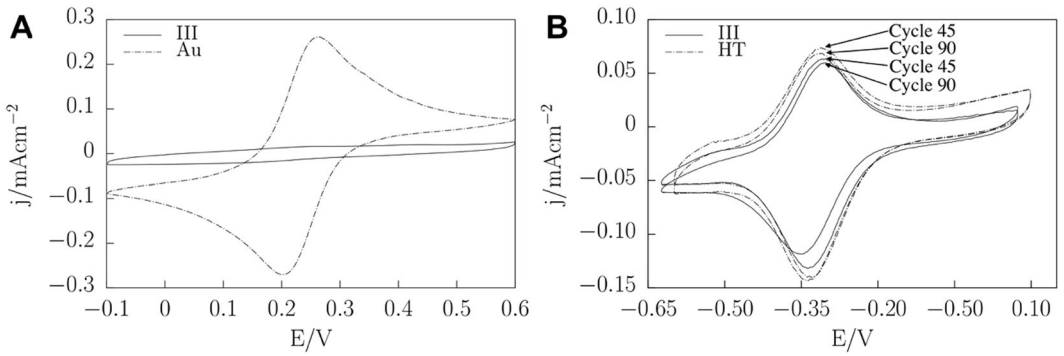

Fig. 6 Comparison between cyclic voltammograms of 1 mM $Fe(CN)_6^{3-/4-}$ at bare Au electrode (dotted line) and coated with SMTF prepared using Method III (solid curve) **a**. Cyclic voltammograms for 0.1 mM $Ru(NH_3)_6^{3+}$, obtained at Au thin film electrodes coated with SMTF prepared using Method HT (dotted curve) and Method III (solid curve) **b**. All experiments were carried out in 0.1 M KCl solution of pH 5 at a scan rate of 0.05 V s^{-1}

CTAB-templated SMTF onto gold can be attributed to bromide ions adsorption onto the gold surface [68, 69].

In order to assess the performance of SMTF as perm-selective membranes, two F127-templated SMTFs were deposited using Methods HT and III onto Si wafers coated with Au thin films and used as working electrodes. Multiple cyclic voltammograms were recorded in a three-electrode cell containing either 1 mM $Fe(CN)_6^{3-/4-}$ or 0.1 mM $Ru(NH_3)_6^{3+}$, which were used as anionic and cationic electrochemical probes, respectively. Representative voltammograms are shown in Fig. 6. In the case of the negatively charged ferrocyanide probe, no discernable electrochemical signal is observed in the SMTF-coated gold electrodes (Fig. 6a). This behavior demonstrates that the silica films are robust and exclude negatively charged ions, as expected in a silica porous surface that bears negative charges in the pH range explored. On the contrary, when using a positively charged probe, a pair of anodic and cathodic peaks between −0.3 and −0.35 V is recorded (Fig. 6b). These peaks can be attributed to the oxidation and reduction of adsorbed $Ru(NH_3)_6^{3+}$ [56]. The peak current is similar for films prepared through calcination or consolidation–extraction, and more than 100 cycles could be recorded on both, with minimum signal losses. The small difference in intensity observed in both types of electrodes can be attributed to the differences in films thickness, porosity, or covered electrode area, taking into account that $Ru(NH_3)_6^{3+}$ tends to preconcentrate in the mesopores.

The chemical and mechanical stability of the bilayer electrode was tested carrying out over 100 electrochemical measurement cycles. A decrease in the peak current is observed with the increasing number of electrochemical cycles, which can be attributed to the progressive dissolution of the silica films [56]; a similar rate of current decrease was observed for both films. These results presented here show that SMTF prepared using Method III are suitable for the development of electrochemical sensors containing a perm-selective component. Detailed studies are underway to shed light into the stability of these low-temperature treated films toward stable perm-selective electrodes. As reported previously, addition of Zr precursors to the initial sol formulation can improve the mechanical and chemical stability of silica-based MTFs [56].

4 Conclusions

A variety of post-synthetic treatment methods were explored and tested with the objective of obtaining continuous, homogeneous SMTF with accessible porous systems and robust inorganic frameworks. The low-temperature treatments developed here allow harnessing silica condensation and phase separation of the template, leading to robust silica frameworks with well-defined, accessible mesopore systems. This is an important step for the inclusion of organic functionalities or even biomolecules in nanofiltration, molecular preconcentrating systems, or perm-selective electrodes that can be deposited onto thermally labile substrates. The comparison of the methods suggests that all of them are suitable for the deposition of well-condensed SMTF with an extraction of the surfactant higher than 85%. However, the porous structure can be highly affected by the post-synthetic treatment and, in this regard, SMTF with a single and uniform system of pores and necks were obtained by the combination of heat treatment at 130 °C in vacuum for 7 days. Finally, to demonstrate the potential of these materials to the field of sensing devices, a proof-of-concept was developed to confirm film stability, accessibility to the electrode surface, and perm-selectivity toward redox probes. The device was working and can be reused for at least 90 electrochemical consecutive cycles in aqueous solutions.

Acknowledgements This work was supported by INTI, INS-UNSAM, and Agencia Nacional de Promoción Científica y Tecnológica (Projects PICT-2015-3526, PICT 2017-4651, and PICT-2018-04236). Dr. M.C. Fuertes is gratefully thanked for the EPAs measurements.

Compliance with ethical standards

Conflict of interest The authors declare that they have no conflict of interest.

Publisher's note Springer Nature remains neutral with regard to jurisdictional claims in published maps and institutional affiliations.

References

1. Serrano E, Linares N, Garcia-Martinez J, Berenguer JR (2013) Sol-gel coordination chemistry: building catalysts from the bottom-up. ChemCatChem 5:844–860. https://doi.org/10.1002/cctc.201200938
2. Brinker CJ, Lu Y, Sellinger A, Fan H (1999) Evaporation-induced self-assembly: nanostructures made easy. Adv Mater 11:579–585. https://doi.org/10.1002/(SICI)1521-4095(199905)11:7<579::AID-ADMA579>3.0.CO;2-R3.0.CO;2
3. Wang J, Ma Q, Wang Y et al. (2018) New insights into the structure-performance relationships of mesoporous materials in analytical science. Chem Soc Rev 47:8766–8803. https://doi.org/10.1039/c8cs00658j
4. Wei J, Sun Z, Luo W et al. (2017) New insight into the synthesis of large-pore ordered mesoporous materials. J Am Chem Soc 139:1706–1713. https://doi.org/10.1021/jacs.6b11411
5. Florek J, Caillard R, Kleitz F (2017) Evaluation of mesoporous silica nanoparticles for oral drug delivery-current status and perspective of MSNs drug carriers. Nanoscale 9:15252–15277. https://doi.org/10.1039/c7nr05762h
6. Walcarius A (2018) Silica-based electrochemical sensors and biosensors: recent trends. Curr Opin Electrochem 10:88–97. https://doi.org/10.1016/j.coelec.2018.03.017
7. Innocenzi P, Malfatti L (2013) Mesoporous thin films: properties and applications. Chem Soc Rev 42:4198–4216. https://doi.org/10.1039/c3cs35377j
8. Laskowski Ł, Laskowska M, Vila N et al. (2019) Mesoporous silica-based materials for electronics-oriented applications. Molecules 24:2395. https://doi.org/10.3390/molecules24132395
9. Etienne M, Zhang L, Vilà N, Walcarius A (2015) Mesoporous materials-based electrochemical enzymatic biosensors. Electroanalysis 27:2028–2054. https://doi.org/10.1002/elan.201500172
10. Vilà N, Walcarius A (2015) Electrochemical response of vertically-aligned, ferrocene-functionalized mesoporous silica films: effect of the supporting electrolyte. Electrochim Acta. https://doi.org/10.1016/j.electacta.2015.02.169
11. Grosso D, Balkenende AR, Albouy PA et al. (2001) Two-dimensional hexagonal mesoporous silica thin films prepared from block copolymers: detailed characterization and formation mechanism. Chem Mater 13:1848–1856. https://doi.org/10.1021/cm001225b
12. Herregods SJF, Mertens M, Van Havenbergh K et al. (2013) Controlling pore size and uniformity of mesoporous titania by early stage low temperature stabilization. J Colloid Interface Sci 391:36–44. https://doi.org/10.1016/j.jcis.2012.07.098
13. Beck JS, Vartuli JC, Roth WJ et al. (1992) A new family of mesoporous molecular sieves prepared with liquid crystal templates. J Am Chem Soc 10834–10843. https://doi.org/10.1021/ja00053a020
14. Kresge CT, Leonowicz ME, Roth WJ et al. (1992) Ordered mesoporous molecular sieves synthesized by a liquid-crystal template mechanism. Nature 359:710–712. https://doi.org/10.1038/359710a0
15. Di Renzo F, Cambon H, Dutartre R (1997) A 28-year-old synthesis of micelle-templated mesoporous silica. Microporous Mater 10:283–286. https://doi.org/10.1016/S0927-6513(97)00028-X
16. Clark T, Ruiz JD, Fan H et al. (2000) A new application of UV-ozone treatment the preparation of substrate-supported, mesoporous thin films. Chem Mater 12:3879–3884. https://doi.org/10.1021/cm000456f
17. Hozumi A, Yokogawa Y, Kameyama T et al. (2000) Photocalcination of mesoporous silica films using vacuum ultraviolet light. Adv Mater 12:985–987. https://doi.org/10.1002/1521-4095(200006)12:13<985::AID-ADMA985>3.0.CO;2-#
18. Huang J, Ichinose I, Kunitake T, Nakao A (2002) Preparation of nanoporous Titania films by surface sol-gel process accompanied by low-temperature oxygen plasma treatment. Langmuir 18:9048–9053. https://doi.org/10.1021/la026091q
19. Zhang J, Palaniappan A, Su X, Tay FEH (2005) Mesoporous silica thin films prepared by argon plasma treatment of sol–gel-derived precursor. Appl Surf Sci 245:304–309. https://doi.org/10.1016/j.apsusc.2004.10.049
20. Horiuchi Y, Ura H, Kamegawa T et al. (2011) Low-temperature synthesis of highly hydrophilic Ti-containing mesoporous silica thin films on polymer substrates by photocatalytic removal of structure-directing agents. J Mater Chem 21:236. https://doi.org/10.1039/c0jm01404d
21. Soler-Illia GJAA, Crepaldi EL, Grosso D et al. (2002) Structural control in self-standing mesostructured silica oriented membranes and xerogels. Chem Commun 2298–2299
22. Cagnol F, Grosso D, Soler-Illia GJAA (2003) Humidity-controlled mesostructuration in CTAB-templated silica thin film processing. The existence of amodulable steady state. J Mater Chem 13:61–66
23. Brinker CJ, Scherer GW (1990) Sol-gel science: the physics and chemistry of sol-gel processing. Academic Press, London
24. Nasir T, Zhang L, Vilà N, et al. (2016) Electrografting of 3-aminopropyltriethoxysilane on a glassy carbon electrode for the improved adhesion of vertically oriented mesoporous silica thin films. Langmuir 32. https://doi.org/10.1021/acs.langmuir.6b00798
25. Soler-Illia GJAA, Innocenzi P (2006) Mesoporous hybrid thin films: the physics and chemistry beneath. Chemistry 12:4478–4494
26. Grosso D, Cagnol F, Soler-Illia GJDAA. et al. (2004) Fundamentals of mesostructuring through evaporation-induced self-assembly. Adv Funct Mater 14. https://doi.org/10.1002/adfm.200305036
27. Soler-Illia GJAA, Angelomé PC, Fuertes MC. et al. (2011) Mesoporous hybrid and nanocomposite thin films. A sol-gel toolbox to create nanoconfined systems with localized chemical properties. J Sol-Gel Sci Technol 57:299–312. https://doi.org/10.1007/s10971-010-2172-2
28. Soler-Illia GJDAA, Sanchez C, Lebeau B, Patarin J (2002) Chemical strategies to design textured materials: from microporous and mesoporous oxides to nanonetworks and hierarchical structures. Chem Rev 102. https://doi.org/10.1021/cr0200062
29. Crepaldi EL, Soler-Illia GJDAA, Grosso D, Sanchez C (2003) Nanocrystallised titania and zirconia mesoporous thin films exhibiting enhanced thermal stability. New J Chem 27. https://doi.org/10.1039/b205497n
30. Crepaldi EL, Soler-Illia GJDAA, Grosso D. et al. (2003) Controlled formation of highly organized mesoporous titania thin films: from mesostructured hybrids to mesoporous nanoanatase TiO_2. J Am Chem Soc 125. https://doi.org/10.1021/ja030070g
31. Soler-Illia GJAA, Angelomé PC, Fuertes MC et al. (2012) Critical aspects in the production of periodically ordered mesoporous titania thin films. Nanoscale 4:2549–2566. https://doi.org/10.1039/c2nr11817c

32. Zhuravlev LT (2000) The surface chemistry of amorphous silica. Zhuravlev model. Colloids Surf A 173:1–38. https://doi.org/10.1016/S0927-7757(00)00556-2
33. Mogilnikov KP, Baklanov MR (2002) Determination of Young's modulus of porous low-k films by ellipsometric porosimetry. Electrochem Solid-State Lett 5:F29. https://doi.org/10.1149/1.1517771
34. Fuertes MC, Colodrero S, Lozano G et al. (2008) Sorption properties of mesoporous multilayer thin films. J Phys Chem C 112:3157–3163. https://doi.org/10.1021/jp710612y
35. Doshi DA, Huesing NK, Lu M et al. (2000) Optically defined multifunctional patterning of photosensitive thin-film silica mesophases. Science 290:107–111. https://doi.org/10.1126/science.290.5489.107
36. Soler-Illia GJAA, Azzaroni O (2011) Multifunctional hybrids by combining ordered mesoporous materials and macromolecular building blocks. Chem Soc Rev 40. https://doi.org/10.1039/c0cs00208a
37. Huo Q, Margolese DI, Stucky GD (1996) Surfactant control of phases in the synthesis of mesoporous silica-based materials. Chem Mater 8:1147–1160. https://doi.org/10.1021/cm960137h
38. Boissiere C, Larbot A, Prouzet E (2000) Synthesis of mesoporous MSU-X materials using. Chem Mater 12:1937–1940. https://doi.org/10.1021/cm001012m
39. Gonzalez Solveyra E, Fuertes MC, Soler-Illia GJAA, Angelomé PC (2017) 2D-SAXS in situ measurements as a tool to study elusive mesoporous phases: the case of p6mm TiO_2. J Phys Chem C 121:3623–3631. https://doi.org/10.1021/acs.jpcc.6b12112
40. Ichinose I, Kunitake T (2002) Wrapping and inclusion of organic molecules with ultrathin, amorphous metal oxide films. Chem Rec 2:339–351. https://doi.org/10.1002/tcr.10032
41. Fischereder A, Martínez-Ricci M, Wolosiuk A et al. Mesoporous ZnS thin films prepared by a nanocasting route. Chem Mater 24:1837–1845. https://doi.org/10.1021/cm300395m
42. Tompkins HG, McGahan WA (1999) Spectroscopic ellipsometry and reflectometry. A user's guide, 1st edn. Wiley-Interscience, New York
43. Boissiere C, Grosso D, Lepoutre S et al. (2005) Porosity and mechanical properties of mesoporous thin films assessed by environmental ellipsometric porosimetry. Langmuir 21:12362–12371. https://doi.org/10.1021/la050981z
44. Fattakhova-Rohlfing D (2007) Ion-permselective pH-switchable mesoporous silica thin layers. Chem Mater 19:1640–1647. https://doi.org/10.1021/cm062389g
45. Calvo A, Fuertes MC, Yameen B et al. (2010) Nanochemistry in confined environments: polyelectrolyte brush-assisted synthesis of gold nanoparticles inside ordered mesoporous thin films. Langmuir 26:5559–5567. https://doi.org/10.1021/la9038304
46. Malfatti L, Bellino MG, Innocenzi P, Soler-Illia GJAA (2009) One-pot route to produce hierarchically porous titania thin films by controlled self-assembly, swelling, and phase separation. Chem Mater 21:2763–2769
47. Thommes M, Kaneko K, Neimark AV et al. (2015) Physisorption of gases, with special reference to the evaluation of surface area and pore size distribution (IUPAC Technical Report). Pure Appl Chem 87:1051–1069. https://doi.org/10.1515/pac-2014-1117
48. Etienne M, Quach A, Grosso D et al. (2007) Molecular transport into mesostructured silica thin films: electrochemical monitoring and comparison between *p6m*, *P6₃/mmc*, and *Pm3n* structures. Chem Mater 19:844–856. https://doi.org/10.1021/cm0625068
49. Thielemann J, Girgsdies F, Schlögl R, Hess C (2011) Pore structure and surface area of silica SBA-15: influence of washing and scale-up. Beilstein J Nanotechnol 2:110–8. https://doi.org/10.3762/bjnano.2.13
50. Groen JC, Peffer LAA, Pérez-Ramírez J (2003) Pore size determination in modified micro- and mesoporous materials. Pitfalls and limitations in gas adsorption data analysis. Microporous Mesoporous Mater 60:1–17. https://doi.org/10.1016/S1387-1811(03)00339-1
51. Gregg SJ, Sing KSW, Salzberg HW (1967) Adsorption surface area and porosity. J Electrochem Soc 114:279C. https://doi.org/10.1149/1.2426447
52. Soler-Illia GJAA, Crepaldi EL, Grosso D et al. (2002) Structural control in self-standing mesostructured silica oriented membranes and xerogels. Chem Commun 20:2298–2299. https://doi.org/10.1039/B207595D
53. Angelomé PC (2008) Films delgados mesoporosos de óxidos metálicos, mixtos e híbridos. Hacia un diseño racional de nanomaterialesfuncionales. Facultad de Ciencias Exactas y Naturales—UBA, Buenos Aires
54. Innocenzi P (2003) Infrared spectroscopy of sol–gel derived silica-based films: a spectra-microstructure overview. J Non-Cryst Solids 316:309–319. https://doi.org/10.1016/S0022-3093(02)01637-X
55. Olsen JE, Shimura F (1989) Infrared reflection spectroscopy of the SiO2-silicon interface. J Appl Phys 66:1353–1358. https://doi.org/10.1063/1.344435
56. Alberti S, Steinberg PY, Giménez G et al. (2019) Chemical stability of mesoporous oxide thin film electrodes under electrochemical cycling: from dissolution to stabilization. Langmuir 35:6279–6287. https://doi.org/10.1021/acs.langmuir.9b00224
57. Mazer J, Walther J (1994) Dissolution kinetics of silica glass as a function of pH between 40 and 85 °C. J Non-Cryst Solids 170:32–45. https://doi.org/10.1016/0022-3093(94)90100-7
58. Niibori Y, Kunita M, Tochiyama O, Chida T (2000) Dissolution rates of amorphous silica in highly alkaline solution. J Nucl Sci Technol 37:349–357. https://doi.org/10.1080/18811248.2000.9714905
59. Gorrepati EA, Wongthahan P, Raha S, Fogler HS (2010) Silica precipitation in acidic solutions: mechanism, pH effect, and salt effect. Langmuir 26:10467–10474. https://doi.org/10.1021/la904685x
60. Lange P, Schnakenberg U, Ullerich S, Schliwinski HJ (1990) Disorder in vitreous SiO_2: the effect of thermal annealing on structural properties. J Appl Phys 68:3532–3537. https://doi.org/10.1063/1.346312
61. Lange P, Windbracke W (1989) Characterization of thermal and deposited thin oxide layers by longitudinal optical-transverse optical excitation in fourier transform IR transmission measurements. Thin Solid Films 174:159–164. https://doi.org/10.1016/0040-6090(89)90885-7
62. Lange P (1989) Evidence for disorder-induced vibrational mode coupling in thin amorphous SiO2 films. J Appl Phys 66:201–204. https://doi.org/10.1063/1.344472
63. Shimizu W, Murakami Y (2010) Microporous silica thin films with low refractive indices and high Young's modulus. ACS Appl Mater Interfaces 2:3128–3133. https://doi.org/10.1021/am100612g
64. Gazoni RM, Bellino MG, Cecilia Fuertes M et al. (2017) Designed nanoparticle–mesoporous multilayer nanocomposites as tunable plasmonic–photonicarchitectures for electromagnetic field enhancement. J Mater Chem C. https://doi.org/10.1039/C6TC05195B
65. Robertson C, Lodge AW, Basa P et al. (2016) Surface modification and porosimetry of vertically aligned hexagonal mesoporous silica films. RSC Adv 6:113432–113441. https://doi.org/10.1039/C6RA23059H
66. Fuertes MC (2009) Materiales funcionales multiescala basados en películas de óxidos mesoporosos. UNSAM, San Martín
67. Brinker CJ, Lu Y, Ganguli R et al. (1997) Continuous formation of supported cubic and hexagonal mesoporous films by sol–gel dip-coating. Nature 389:364–368. https://doi.org/10.1038/38699
68. Cheng W, Dong S, Wang E (2003) Synthesis and self-assembly of cetyltrimethylammonium bromide-capped gold nanoparticles. Langmuir 19:9434–9439. https://doi.org/10.1021/la034818k
69. Smith DK, Korgel BA (2008) The importance of the CTAB surfactant on the colloidal seed-mediated synthesis of gold nanorods. Langmuir 24:644–649. https://doi.org/10.1021/la703625a